August 11, 1982 ANL FRA-TM-143

Validation of Alternative Methods and Data for a Benchmark Fast Reactor Depletion Calculation

by

B. J. Toppel, C. H. Adams, R. D. Lawrence, H. Henryson II, K. L. Derstine

Applied Physics Division
Argonne National Laboratory
Argonne, Illinois 60439

FRA TECHNICAL MEMORANDUM NO. 143

Results reported in the FRA-TM series of memoranda frequently are preliminary and subject to revision. Consequently they should not be quoted or referenced without the author's permission.

Work supported by the U. S. Department of Energy.

Validation of Alternative Methods and Data for a Benchmark Fast Reactor Depletion Calculation

by

B. J. Toppel, C. H. Adams, R. D. Lawrence, H. Henryson II, K. L. Derstine

Applied Physics Division
Argonne National Laboratory
Argonne, Illinois 60439

FRA TECHNICAL MEMORANDUM NO. 143

Work supported by the U. S. Department of Energy.

Table of Contents

List of Figures

List of Tables

VALIDATION OF ALTERNATIVE METHODS AND DATA FOR A BENCHMARK FAST REACTOR DEPLETION CALCULATION*

B. J. Toppel, C. H. Adams, R. D. Lawrence, H. Henryson II, K. L. Derstine
Argonne National Laboratory
Applied Physics Division
9700 South Cass Avenue
Argonne, Illinois 60439

ABSTRACT

Alternative neutronics models, data processing procedures, and data bases have been used to examine two 383.5 day burn cycles for a 1000 MWe heterogeneous LMFBR design developed by the Large Core Code Evaluation Working Group (LCCEWG). The diffusion theory neutronics methods used are finite difference, nodal, and spatial flux synthesis. Four, eight, and twenty-group multigroup cross sections based on ENDF/B-IV and ENDF/B-V data bases are compared. The effect of parked control rods as compared with rods moving during the burn cycles is examined. Various performance parameters are compared including burnup reactivity swings, rod worths, fuel burnup, power splits, and sodium void reactivity effects. The sensitivity of the results to choices in the modeling process are discussed.

INTRODUCTION

Benchmark analysis has traditionally been an important means of qualifying methods, codes and data for reactor physics applications. In this study an attempt is made to quantify the effects of alternative neutronics models, data processing assumptions, and data bases upon the calculated performance characteristics of an LMFBR. The current study differs from the work of other benchmark efforts in that self-consistency among alternative models is emphasized and the impact of both data and methods are addressed in a single benchmark study.

The codes which were used in the study have been developed at Argonne National Laboratory by the authors. This permits a particularly meaningful intercomparison since any bias toward a particular methodology is removed. The three methods which were investigated span the range of those which are generally considered for three-dimensional diffusion-theory reactor depletion studies: finite difference, nodal and spatial flux synthesis. Each has its own advantages and disadvantages. The finite-difference method is well-known and generally considered a standard for such applications but is limited in three-dimensional applications because of long computation times. Although recently developed nodal methods have demonstrated high accuracy in very short running times for light water reactor analyses in Cartesian geometry, relatively little work has been done on the extension of these methods to fast reactor calculations in hexagonal geometry. The spatial flux-synthesis methods are efficient and accurate for fast reactor calculations but it is difficult to assess the accuracy of a particular calculation because of the dependence on the trial function selection.

*Work performed under the auspices of the U.S. Department of Energy

DESCRIPTION OF THE CALCULATIONAL MODEL

The reactor model chosen for the study is a 1000 MWe heterogeneous design which was developed by the Large Core Code Evaluation Working Group (LCCEWG) for benchmark intercomparisons.[1]

The benchmark calculations were performed using a three-dimensional model with 60° symmetry in the plane. Fig. 1 shows the arrangement of a typical plane and indicates the placement of the three driver zones, the three internal blanket zones, the radial blanket and shield, and the various control-rod positions. The lattice pitch is 16.33 cm. The fuel batch loading sequence is also indicated.

Figure 2, which is an R-Z representation of the reactor, is presented merely to indicate the axial dimensions of the model. No actual R-Z calculations were performed owing to the necessarily arbitrary nature of such an R-Z representation. The axial mesh used is given in Table 1.

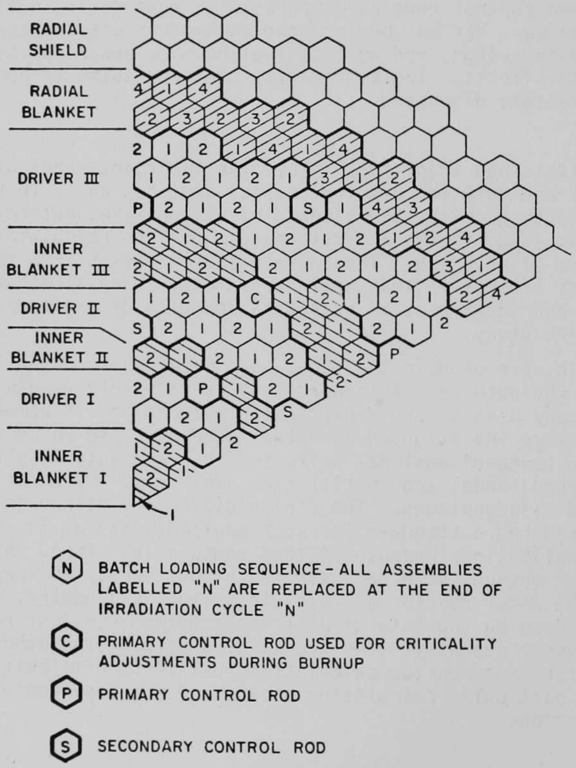

FIGURE 1. SIXTY DEGREE SECTOR OF CORE LAYOUT

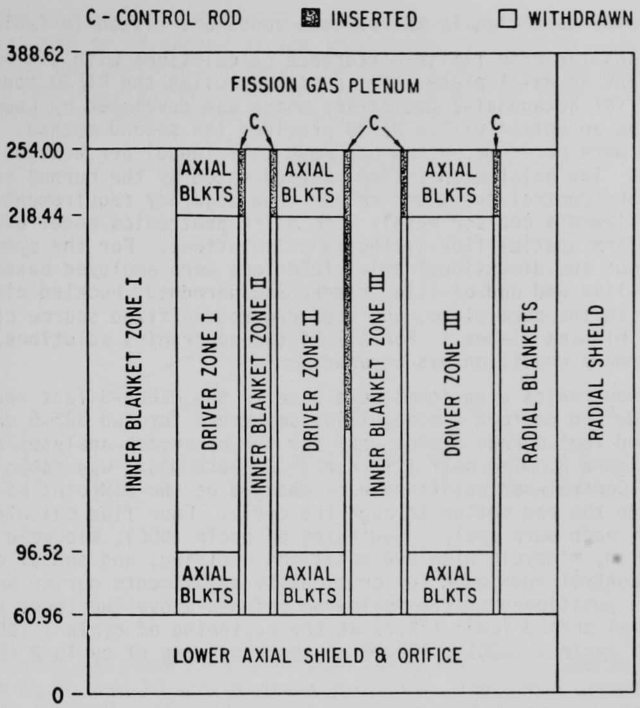

FIGURE 2. REACTOR DIAGRAM INDICATING AXIAL DIMENSIONS

Table 1. Axial Definition Used in the Benchmark Calculations

Axial Range (cm)	Number of Axial Regions	Number of Mesh Intervals: Finite Difference and Spatial Synthesis	Number of Mesh Intervals: Nodal
0 - 60.96	1	2	1
60.96 - 96.52	2	6	2
96.52 - 218.44	8	24	11
218.44 - 254.0	2	6	2
254.0 - 388.62	1	4	1

The initial atom densities in the various zones are listed in Table 2.

Standard triangular-mesh finite-difference calculations with six mesh points per hexagon and 42 axial planes were performed using the DIF3D code.[2] A new nodal scheme for hexagonal-Z geometries which was developed by Lawrence[3] and implemented as an option within DIF3D provided the second method. The nodal calculations were performed using one mesh cell (node) per hexagon and 17 axial planes. The axial mesh (~15cm) was dictated by the burnup region definitions and control positions rather than accuracy requirements (which would have allowed a coarser mesh). The third neutronics model used the SYN3D code[4] to perform spatial flux-synthesis calculations. For the synthesis calculations various two-dimensional trial functions were employed based upon beginning-of-life and end-of-life, rodded and unrodded, buckled eigenvalue calculations in the core plane, and rodded/unrodded fixed source calculations in the axial blanket planes.[5] For all of the neutronics solutions, a vacuum external boundary condition was assumed.

The various neutronics algorithms were used in the REBUS-3 fast reactor depletion code[6] to perform a nonequilibrium burnup for two 383.5 day cycles. The simplified fuel burnup chains used for the benchmark analyses are indicated in Figure 3. The half life for ^{241}Pu beta decay was taken to be 14.4 years. Control-rod positions were changed at the midpoint of each cycle to approximate the rod motion through the cycle. Four flux calculations were performed for each burn cycle: beginning of cycle (BOC), midcycle with rods at BOC position, midcycle with rod positions modified, and end of cycle (EOC). The primary control rods used for criticality adjustments during burnup (Fig. 1) were positioned at the following heights above the lower surface of the lower axial shield (cm); 172.72 at the beginning of cycle 1 (BOC1); 193.04 at the end of cycle 1 (EOC1); 182.88 at the beginning of cycle 2 (BOC2); and

Table 2. Initial Atom-Densities (atoms/barn-cm)

	Driver	Internal or Radial Blanket	Radial Shield Structure	Control[a]	Na Channel[b]	Axial Blanket	Fission Gas Plenum	Lower Axial Shield
U-235	1.9168-5[c]	2.9907-5	0.0	0.0	0.0	2.7953-5	0.0	0.0
U-238	8.6912-3	1.3558-2	0.0	0.0	0.0	1.2673-2	0.0	0.0
Pu-239	1.3591-3	0.0	0.0	0.0	0.0	0.0	0.0	0.0
Pu-240	4.0789-4	0.0	0.0	0.0	0.0	0.0	0.0	0.0
Pu-241	2.0392-4	0.0	0.0	0.0	0.0	0.0	0.0	0.0
Pu-242	4.8481-5	0.0	0.0	0.0	0.0	0.0	0.0	0.0
Cr	2.8111-3	2.3756-3	1.3180-2	3.1030-3	1.3980-3	2.8111-3	2.5335-3	1.2280-2
Fe	9.6814-3	8.1994-3	4.5410-2	1.0690-2	4.8170-3	9.6814-3	8.7337-3	4.2290-2
Ni	1.9207-3	1.6266-3	9.0060-3	2.1200-3	9.5520-4	1.9207-3	1.7326-3	8.3900-3
Mo	2.1764-4	1.8431-4	1.0210-3	2.4030-4	1.0820-4	2.1764-4	1.9633-4	9.5070-4
Mn	2.6609-4	2.2528-4	1.2480-3	2.9370-4	1.3240-4	2.6609-4	2.4001-4	1.1620-3
Na	8.2217-3	6.2401-3	2.2370-3	1.0490-3	1.8420-2	8.2217-3	7.8509-3	3.9930-3
O	2.1460-2	2.7176-2	0.0	0.0	0.0	2.1460-2	0.0	0.0
F.P.	0.0	0.0	0.0	0.0	0.0	0.0	0.0	0.0
B-10	0.0	0.0	0.0	2.9110-2	0.0	0.0	0.0	0.0
B-11	0.0	0.0	0.0	2.5310-3	0.0	0.0	0.0	0.0
C	0.0	0.0	0.0	8.2700-3	0.0	0.0	0.0	0.0

[a]Control assembly inserted

[b]Control assembly withdrawn

[c]Read as 1.9168×10^{-5}

198.12 at the end of cycle 2 (EOC2). All other primary and secondary control rods were assumed to be parked at the upper axial blanket/driver interface. Fuel shuffling was performed between the first and second cycles as indicated in Fig. 1. The calculations assumed a reactor power of 2740 MWth and a refueling interval of 383.5 effective full power days.

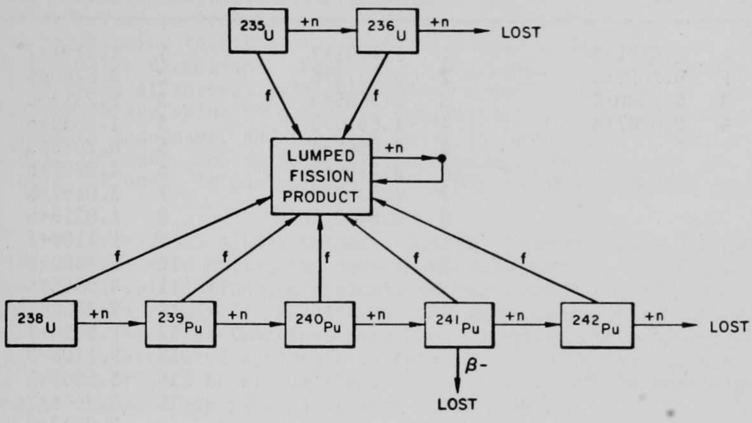

FIGURE 3. FUEL BURNUP CHAINS FOR THE BENCHMARK ANALYSES

Multigroup cross sections were generated using the MC^2-2[7] and MC^2-2/SDX codes[8,9] in 4, 8, and 20 energy group versions. The group structures are indicated in Table 3. Separate cross sections were generated for each driver zone and inner blanket zone, and for the radial blanket, radial shield, axial blankets, lower axial shield, fission gas plenum, and control channels. Pin heterogeneity effects were modeled for all of the driver and blanket fuel assemblies.

Cross sections were generated from both the ENDF/B-IV[10] and ENDF/B-V[11] data bases, and also separate cross sections were prepared with sodium voided from the driver and blanket zones for use in the sodium void reactivity worth calculations. A single lumped fission product was used in the depletion calculations with cross sections based upon the ENDF/B-V fission product data files.[12]

DESCRIPTION OF NEUTRONICS METHODS

The reference calculations utilized the 8 energy group cross sections based on the ENDFB-V data. The DIF3D/REBUS-3 calculations used standard triangular-mesh finite difference with six mesh points per hexagon and 42 axial planes as indicated in Table 1. The finite difference equations employed by DIF3D are mesh centered.

The nodal option in DIF3D solves the neutron diffusion equation using 1 mesh cell (node) per hexagonal assembly. The nodal equations are derived using higher order polynomial approximations[3] to the spatial dependence of the flux within the hexagonal node. The final equations involve spatial moments of the flux within the node plus face-averaged partial currents across the surfaces

Table 3. Broad Group Energy Structures

Four Group: Group	Four Group: Upper Energy (eV)	Eight Group: Group	Eight Group: Upper Energy (eV)	Twenty Group: Group	Twenty Group: Upper Energy (eV)
1	1.4191+7*	1	1.4191+7	1	1.4191+7
2	8.2085+5	2	2.2313+6	2	3.6788+6
3	6.7380+4	3	8.2085+5	3	2.2313+6
4	2.0347+3	4	1.8316+5	4	1.3534+6
		5	4.0868+4	5	8.2085+5
		6	9.1188+3	6	4.9787+5
		7	2.0347+3	7	3.0197+5
		8	4.5400+2	8	1.8316+5
				9	1.1109+5
				10	6.7380+4
				11	4.0868+4
				12	2.4788+4
				13	1.5034+4
				14	9.1188+3
				15	5.5309+3
				16	3.3546+3
				17	2.0347+3
				18	1.2341+3
				19	7.4852+2
				20	4.5400+2

*Read as 1.4191 $\times 10^7$

of the node. The three-dimensional method involves a total of 13 unknowns per group per node: 8 outgoing partial currents (1 on each of the 8 surfaces) plus 5 flux moments (the node-averaged flux, plus one spatial moment in each of the three hex-plane directions and the axial direction). Although the DIF3D finite-difference method using six triangles per hexagon involves only six unknowns per hexagon for each axial mesh interval, the nodal option is considerably faster. This is because the solution of the partial current equations typically requires only 2 inner iterations per group, while the solution of the 6 triangle-per-hexagon finite-difference equations often requires 5 to 10 inner iterations; consequently, for two-dimensional problems, the nodal method requires 2 to 3 times less CPU time than the finite-difference calculation. In addition, for three-dimensional calculations, the higher order axial approximation in the nodal scheme permits the use of an axial mesh which is at least 4 times coarser than that used in typical finite-difference calculations. This decrease in the number of axial planes yields additional factors of 2 to 3 reduction in CPU time, thus giving overall CPU time ratios of between 4 and 9 for three-dimensional problems, depending upon the desired solution accuracy and whether the axial zone boundaries permit full advantage to be taken of the nodal coarse-mesh capabilities. For the reference nodal option DIF3D/REBUS-3, 17 axial planes were used as indicated in Table 1.

One drawback of the nodal approach is the lack of information concerning the spatial distribution of the flux within the node. A simple procedure is used in the nodal option of DIF3D to compute more accurate peak power densities and fluxes than those obtained by sampling only the node-averaged values. In two dimensions, this procedure involves sampling surface-averaged fluxes on the six surfaces of the hexagon; the surface fluxes are readily obtained from the calculated interface partial currents. This procedure is extended to three dimensions by assuming that the flux within the node is separable in the hex-plane and axial directions. Peak values are computed by evaluating this assumed flux shape at several axial elevations within the node. If the computed peak-to-average value in a node is unrealistically high, the separability approximation is abandoned, and the peak value in that node is computed by sampling only the node- and surface-averaged values. This "fixup" has been required only for nodes in control assemblies for the test problems studied to date.

The SYN3D code provides a single-channel, spatial flux-synthesis approximation to the finite difference multigroup neutron-diffusion-theory equations. For three-dimensional calculations, precalculated two-dimensional expansion or trial functions are required. Relatively straight-forward prescriptions for determination of the trial functions have been developed which reduce the uncertainty associated with synthesis calculations.[5] Nevertheless the arbitrary nature of such trial functions makes it difficult to make a general assessment of the accuracy of a particular calculation.

COMPARISON OF REFERENCE CALCULATIONS

Table 4 compares calculated reactivity swings due to burnup and control rod movement as well as various integral parameters for the three reference methods. Excellent agreement is observed among the three methodologies for power fraction through the cycle, and core peaking factors. Such agreement suggests that the trial functions chosen for the synthesis calculations are appropriate for depletion analysis. The synthesis calculation, however, significantly overpredicts the control rod worth. The Table 4 results also demonstrate a bias in the eigenvalue, burnup reactivity swing, and blanket peaking results between the finite-difference methods and the nodal calculation. The nodal eigenvalues are .3 to .4% lower than the finite-difference results whereas the blanket peaking and burnup are significantly higher. The nodal calculation gives a smaller burnup reactivity swing than the finite-difference results which is related to the plutonium buildup in the internal blankets.

In order to resolve these discrepancies, calculations were made using a previously available four group-cross section set comparing DIF3D/REBUS-3 with 6 and 24 triangles per hexagon and the nodal option DIF3D/REBUS-3 for the first half of the first burn cycle of this benchmark study. Table 5 compares the beginning of cycle 1 (BOC1) and middle of cycle 1 (MOC1) k_{eff} as well as the BOC1 peak power densities. Richardson extrapolation of the finite difference results given in Table 5 shows that the eigenvalues calculated using the nodal option are more accurate than either of the finite-difference calculations. This conclusion is supported by more detailed analysis[13] of a very similar BOC1 configuration which showed that the zero-mesh corrections to the 6 triangles per hexagon eigenvalue are ~-0.4% in the plane and ~-0.1% in the axial direction. This same study[13] also showed that the average fluxes in the inner

Table 4. Comparison of Reference Calculational Methods Using 8 Energy Groups Based on ENDF/B-V

	Finite Difference	Nodal Option	Synthesis[a]
k_{eff} (BOC1)	1.00074	0.99685	1.00054
k_{eff} (BOC1) - k_{eff} (MOC1)	0.0048	0.0042	0.0046
Rod Δk_{eff} (MOC1)[b]	0.0054	0.0056	0.0094
k_{eff} (MOC1) - k_{eff} (EOC1)	0.0021	0.0014	0.0022
k_{eff} (BOC2)[d]	1.00162	0.99851	1.00254
k_{eff} (BOC2) - k_{eff} (MOC2)	0.0025	0.0019	0.0025
Rod Δk_{eff} (MOC2)[c]	0.0033	0.0034	0.0050
k_{eff} (MOC2) - k_{eff} (EOC2)	0.0011	0.0005	0.0012
BOC1			
Power Fraction (%)			
Inner Core	11.9	11.8	11.9
Middle Core	23.8	23.4	23.7
Outer Core	55.2	55.6	55.5
Peak/Average Power			
Inner Core	1.40	1.43	1.38
Middle Core	1.60	1.62	1.62
Outer Core	1.60	1.60	1.62
Total Core	1.62	1.63	1.64
Inner Blankets	3.15	3.82	3.16
Radial Blanket	5.87	7.53	5.81
Breeding Ratio	1.518	1.525	1.518
EOC2			
Average Burnup (MWD/mT)			
Total Core	5.46+4[e]	5.44+4	5.48+4
Inner Blankets	6.45+3	6.56+3	6.45+3
Peak Burnup (MWd/mT)			
Total Core	9.83+4	9.85+4	9.70+4
Inner Blanket	2.45+4	2.57+4	2.37+4
Power Fraction (%)			
Inner Core	13.8	13.8	13.3
Middle Core	25.4	25.3	25.3
Outer Core	39.8	39.6	40.4
Inner Blankets	15.2	15.4	15.0
Peak/Average Power			
Inner Core	1.37	1.38	1.37
Middle Core	1.49	1.50	1.48
Outer Core	1.69	1.70	1.67
Total Core	1.80	1.81	1.77
Inner Blankets	3.80	3.92	3.68
Radial Blanket	5.17	6.16	4.99
Breeding Ratio	1.428	1.429	1.430

[a]Using BOC1 + EOC1 trial functions for cycle 1 and BOC2 + EOC2 trial functions for cycle 2.

[b]Rods moved from 172.72 cm to 193.04 cm.

[c]Rods moved from 182.88 cm to 198.12 cm.

[d]Fuel shuffled and rods moved from 193.04 cm to 182.88 cm.

[e]Read as 5.46×10^4.

Table 5. Comparison of Finite Difference Mesh Refinement with the Nodal Option*

	6Δ per hex	24Δ per hex	Nodal Option
k_{eff} (BOC1)	1.00468	1.00126	1.00074
k_{eff} (MOC1)	0.99979	0.99706	0.99648
k_{eff} (BOC1) - k_{eff} (MOC1)	0.00489	0.00420	0.00426
BOC1			
Peak Power Density (watts/cc)			
Total Core	529.1	528.9	530.0
Inner Blankets	80.5	91.1	97.7
Radial Blankets	63.7	74.0	83.8
Neutronics CPU Time**, sec. for BOC1	419.	2192.	79.

*Calculations performed with a previously available 4 group cross section set
**On the IBM 3033

blankets are under-predicted in the 6 triangles per hexagon calculation, thus explaining the smaller breeding ratios and inner blanket burnups and larger reactivity swings calculated using the finite-difference option.

Comparison of the peak power densities given in Table 5 provides an explanation for the differences in the peak/average powers in the inner and radial blankets seen in Table 4. It is clear that the nodal results are more accurate than the finite-difference results simply because the nodal scheme samples the flux shape at the peak location at the core-blanket interface, while the mesh-centered finite-difference method must use successively refined spatial meshes in order to force mesh points closer to this peak location. Good agreement is observed when the finite-difference peak values are computed by sampling the surface fluxes which are readily calculated from the available mesh-centered fluxes.

Finally, the CPU times given in Table 5 demonstrate that the improved accuracy of the nodal option is obtained in significantly reduced CPU times relative to the finite-difference option.

PARKED CONTROL RODS

To assess the impact of the control rod movement during the burnup cycles, two additional nodal option DIF3D/REBUS-3 calculations were run with the eight group cross section set. In the first of these the rods C (Fig. 1) were parked for the entire calculation at a height of 187.96 cm., and for the second, at 218.44 cm., the core-upper axial blanket interface (see Fig. 2).

Table 6 compares the two parked-rod calculations with the reference model calculation involving normal rod movement.

It is obvious from these data that the control rod position assumed for the depletion calculation has very little impact on the computational results. If generally applicable, such a conclusion leads to a considerable simplification

TABLE 6. Comparison of Parked Control Rods with Rod Movement for the Nodal Option Neutronics Method Using 8 Groups and ENDF/B-V

	Reference	Rods Parked at 187.96 cm	Rods Parked at 218.44 cm
k_{eff} (BOC1)	0.99685	1.00060	1.00458
k_{eff} (BOC1) - k_{eff} (MOC1)	0.0042	0.0037	0.0032
Rod Δk_{eff} (MOC1)[a]	0.0056	-	-
k_{eff} (MOC1) - k_{eff} (EOC1)	0.0014	0.0015	0.0014
k_{eff} (BOC2)[b]	0.99851	0.99968	1.00366
k_{eff} (BOC2) - k_{eff} (MOC2)	0.0019	0.0018	0.0016
Rod Δk_{eff} (MOC2)[c]	0.0034	-	-
k_{eff} (MOC2) - k_{eff} (EOC2)	0.0005	0.0006	0.0005
BOC1			
Power Fraction (%)			
Inner Core	11.8	12.0	12.1
Middle Core	23.4	24.6	25.7
Outer Core	55.6	54.3	53.1
Peak/Average Power			
Inner Core	1.43	1.44	1.44
Middle Core	1.62	1.60	1.57
Outer Core	1.60	1.64	1.66
Total Core	1.63	1.63	1.66
Inner Blankets	3.82	3.79	3.80
Breeding Ratio	1.525	1.523	1.525
EOC2			
Average Burnup (MWd/mT)			
Total Core	5.44+4[d]	5.44+4	5.45+4
Inner Blankets	6.56+3	6.57+3	6.59+3
Peak Burnup (MWd/mT)			
Total Core	9.85+4	9.90+4	9.81+4
Inner Blankets	2.57+4	2.60+4	2.52+4
Power Fraction (%)			
Inner Core	13.8	14.0	13.6
Middle Core	25.3	25.1	25.5
Outer Core	39.6	39.7	39.8
Inner Blankets	15.4	15.4	15.4
Peak/Average Power			
Inner Core	1.38	1.37	1.38
Middle Core	1.50	1.51	1.48
Outer Core	1.70	1.68	1.70
Total Core	1.81	1.82	1.80
Inner Blankets	3.92	3.95	3.83
Breeding Ratio	1.429	1.430	1.431

[a]Rods moved from 172.77 cm to 193.04 cm.

[b]Fuel shuffled and rods moved from 193.04 cm to 182.88 cm.

[c]Rods moved from 182.88 cm to 198.12 cm.

[d]Read as 5.44×10^4.

in LMFBR depletion analysis since one need not determine average control rod positions through the burn cycle but may rely upon calculations which park all control at the EOC position, the core-axial blanket interface. This conclusion might be biased by the fact that the greatest insertion of control in the reference calculation is only 18 inches into the 48 inch core. However, heterogeneous core designs generally have small reactivity swings which in large measure determines the control positions. Thus it would seem that reliable depletion calculations can be performed for heterogeneous fast reactor problems by assuming that control rods are positioned at the core-axial blanket interface throughout the burn.

EFFECT OF MULTIGROUP CROSS SECTION ENERGY DETAIL AND DATA BASE

The nodal option DIF3D/REBUS-3 calculation was repeated using the four-group cross section structure (see Table 3) and with the eight-group structure using the ENDF/B-IV data base. Table 7 compares the reactivity swings due to burnup and rod movement and the various integral parameters with the reference nodal calculation.

It is clear that the four- and eight-group results are in excellent agreement for all parameters. Thus it is possible to significantly reduce computing costs for such depletion analysis by a reduction in the number of energy groups provided that sufficient spatial detail is incorporated into the cross section preparation. As noted above, the cross section sets prepared for the benchmark analysis included spatial collapsing over each reactor zone and thus accounted for variations in the spectral dependence of the flux in detail. If such spatial detail had not been incorporated into the cross-section preparation, equivalent agreement would not have been found. For example, a calculation using only one set of core and internal-blanket cross sections gave a BOC1 eight-group inner-blanket peaking factor of 3.80 whereas the equivalent four-group result was 2.88.

The data of Table 7 also show that there is very good agreement between the results obtained with ENDF/B-IV and ENDF/B-V data. It should be noted, however, that both sets of calculations made use of the same ENDF/B-V lumped fission product. The lower k_{eff} values given in Table 7 with ENDF/B-IV data are typical of dilute LMFBR systems and can be attributed in large measure to increases in $\bar{\nu}$ and σ_f of ^{239}Pu in going to ENDF/B-V. Clearly the k_{eff} bias between the datasets would impact upon enrichment determinations and hence equilibrium cycle depletion analysis unless something were done to account for the effect.

THE INFLUENCE OF TRIAL FUNCTIONS ON THE FLUX-SYNTHESIS RESULTS

Synthesis trial functions were generated using the 2D model shown in Fig. 1, with DIF3D/REBUS-3 performing the two-cycle burnup at a power level of 22.042 MWth, which corresponds to the core average linear power.[1] Functions were saved at BOC1, EOC1, BOC2 and EOC2 for primary rods C inserted and withdrawn. Bucklings of 0.0004 cm^{-1} for rodded calculations and 0.0005 cm^{-1} for unrodded calculations were applied to achieve roughly the critical eigenvalue. Rodded and unrodded BOC1 axial-blanket trial functions were obtained from fixed source calculations of the type described in Reference 5.

Table 8 compares the results of three burnup calculations using SYN3D (with different choices of trial functions) with the calculation which used the finite-difference code DIF3D. The reference SYN3D/REBUS-3 trial-function set

TABLE 7. Comparison of Energy Group Structures and Data Bases for the Nodal Option Neutronics Method

	ENDFB-V		ENDFB-IV
	8 Groups	4 Groups	8 Groups
k_{eff} (BOC1)	0.99685	0.99841	0.98996
k_{eff} (BOC1) - k_{eff} (MOC1)	0.0042	0.0048	0.0042
Rod Δk_{eff} (MOC1)[a]	0.0056	0.0058	0.0057
k_{eff} (MOC1) - k_{eff} (EOC1)	0.0014	0.0018	0.0013
k_{eff} (BOC2)[b]	0.99851	0.99959	0.99164
k_{eff} (BOC2) - k_{eff} (MOC2)	0.0019	0.0023	0.0018
Rod Δk_{eff} (MOC2)[c]	0.0034	0.0036	0.0035
k_{eff} (MOC2) - k_{eff} (EOC2)	0.0005	0.0009	0.0004
BOC1			
Power Fraction (%)			
Inner Core	11.8	11.8	11.6
Middle Core	23.4	23.4	23.2
Outer Core	55.6	55.7	55.9
Peak/Average Power			
Inner Core	1.43	1.43	1.43
Middle Core	1.62	1.62	1.62
Outer Core	1.60	1.60	1.60
Total Core	1.63	1.63	1.64
Inner Blankets	3.82	3.81	3.86
Breeding Ratio	1.525	1.518	1.528
EOC2			
Average Burnup (MWd/mT)			
Total Core	5.44+4[d]	5.45+4	5.44+4
Inner Blankets	6.56+3	6.48+3	6.56+3
Peak Burnup (MWd/mT)			
Total Core	9.85+4	9.81+4	9.85+4
Inner Blankets	2.57+4	2.53+4	2.57+4
Power Fraction (%)			
Inner Core	13.8	13.7	13.8
Middle Core	25.3	25.2	25.4
Outer Core	39.6	39.9	39.6
Inner Blankets	15.4	15.2	15.4
Peak/Average Power			
Inner Core	1.38	1.38	1.38
Middle Core	1.50	1.50	1.50
Outer Core	1.70	1.69	1.70
Total Core	1.81	1.80	1.81
Inner Blankets	3.92	3.90	3.92
Breeding Ratio	1.429	1.425	1.432

[a]Rods moved from 172.72 cm to 193.04 cm.

[b]Fuel shuffled and rods moved from 193.04 cm to 182.88 cm.

[c]Rods moved from 182.88 cm to 198.12 cm.

[d]Read as 5.44×10^4.

TABLE 8. Comparison of Trial Functions for the Spatial Synthesis Neutronics Method Using 8 Energy Groups and ENDF/B-V

Trial Functions Used	BOC1 + EOC1 for Cycle 1 BOC2 + EOC2 for Cycle 2	BOC1 + EOC2	BOC1	Finite Difference
k_{eff} (BOC1)	1.00054	1.00053	0.99989	1.00074
k_{eff} (BOC1) - k_{eff} (MOC1)	0.0046	0.0050	0.0117	0.0048
Rod Δk_{eff} (MOC1)[a]	0.0094	0.0092	0.0095	0.0054
k_{eff} (MOC1) - k_{eff} (EOC1)	0.0022	0.0026	0.0094	0.0021
k_{eff} (BOC2)[b]	1.00254	1.00386	0.99477	1.00162
k_{eff} (BOC2) - k_{eff} (MOC2)	0.0025	0.0030	0.0103	0.0025
Rod Δk_{eff} (MOC2)[c]	0.0050	0.0049	0.0054	0.0033
k_{eff} (MOC2) - k_{eff} (EOC2)	0.0012	0.0019	0.0088	0.0011
BOC1				
Power Fraction (%)				
Inner Core	11.9	12.0	11.4	11.9
Middle Core	23.7	23.7	23.0	23.8
Outer Core	55.5	55.4	56.7	55.2
Peak/Average Power				
Inner Core	1.38	1.38	1.44	1.40
Middle Core	1.62	1.62	1.66	1.60
Outer Core	1.62	1.62	1.58	1.60
Total Core	1.64	1.64	1.64	1.62
Inner Blankets	3.16	3.16	3.18	3.15
Breeding Ratio	1.518	1.518	1.517	1.518
EOC1				
Average Burnup (MWd/mT)				
Total Core	2.79+4[d]	2.79+4	2.80+4	2.78+4
Inner Blankets	2.63+3	2.61+3	2.34+3	2.62+3
Peak Burnup (MWd/mT)				
Total Core	4.97+4	4.85+4	4.59+4	5.00+4
Inner Blankets	9.28+3	8.93+3	7.91+3	9.84+3
Power Fraction (%)				
Inner Core	13.2	13.1	11.0	13.7
Middle Core	26.4	25.8	23.6	26.4
Outer Core	43.2	43.9	49.3	42.7
Inner Blankets	12.0	11.9	10.3	12.1
Peak/Average Power				
Inner Core	1.36	1.35	1.37	1.36
Middle Core	1.49	1.48	1.56	1.51
Outer Core	1.68	1.65	1.63	1.69
Total Core	1.78	1.74	1.64	1.80
Inner Blankets	3.53	3.42	3.38	3.62
Breeding Ratio	1.469	1.471	1.459	1.466
EOC2				
Average Burnup (MWd/mT)				
Total Core	5.48+4	5.48+4	5.54+4	5.46+4
Inner Blankets	6.45+3	6.46+3	5.56+3	6.45+3
Peak Burnup (MWd/mT)				
Total Core	9.70+4	9.64+4	9.09+4	9.83+4
Inner Blankets	2.37+4	2.37+4	1.85+4	2.45+4
Power Fraction (%)				
Inner Core	13.3	13.3	10.6	13.8
Middle Core	25.3	25.2	22.7	25.4
Outer Core	40.4	40.6	47.5	39.8
Inner Blankets	15.0	15.0	12.4	15.2
Peak/Average Power				
Inner Core	1.37	1.37	1.38	1.37
Middle Core	1.48	1.47	1.56	1.49
Outer Core	1.67	1.67	1.63	1.69
Total Core	1.77	1.76	1.64	1.80
Inner Blankets	3.68	3.67	3.33	3.80
Breeding Ratio	1.430	1.430	1.418	1.428

[a] Rods moved from 172.72 cm to 193.04 cm.

[b] Fuel shuffled and rods moved from 193.04 cm to 182.88 cm.

[c] Rods moved from 182.88 cm to 198.12 cm.

[d] Read as 2.79×10^4.

consisted of six fluxes: rodded and unrodded BOC axial blanket functions plus rodded and unrodded, BOC and EOC core eigenvalue functions within each burn cycle. The core functions in this first set were changed between cycles. The second set also contained six functions, but the core functions were generated at the beginning of the first cycle (BOC1) and the end of the second (EOC2). This set was not changed between cycles. The third set contained four trial functions; rodded and unrodded BOC1 core functions and rodded and unrodded BOC axial blanket functions were used throughout both cycles.

In all three SYN3D/REBUS-3 calculations trial-function zoning was used to reduce running time. Rodded blanket functions were applied only in the top half of the model, and unrodded blanket functions were used only in the lower half. The switch was made at 142.24 cm. Rodded core functions were used in the core, upper blanket and plenum. Unrodded core functions were used in the core, lower blanket and lower shield.

For the most part Table 8 shows the SYN3D/REBUS-3 results to be in good agreement with the DIF3D/REBUS-3 calculation. There is a substantial difference in rod worth for both cycles, but power fractions and core peak-to-average powers tend to agree to within 2%. Peak burnup figures agree well for the core. There are errors as high as 3-4% in some of the peak burnups and peaking factors in the inner blankets.

The differences between SYN3D/REBUS-3 and DIF3D/REBUS-3 in general are somewhat larger for the other two trial-functions sets. Errors are particularly obvious in inner-blanket results and power fractions for the set that only used BOC fluxes (the third set). On the other hand, the reference set, which switches functions between cycles, shows only a small improvement in accuracy over the second set.

REACTIVITY EFFECT OF SODIUM VOIDING

The VARI3D Code[14] was used to analyze the components of the reactivity effect due to voiding sodium from the three core driver zones and the corresponding upper axial blankets. Exact perturbation theory was used in that the real flux was obtained before the sodium voiding and the adjoint solution corresponded to the voided configuration. The atom densities used were generated by the reference 8 group finite difference calculations.

The isotopic concentrations were obtained from the DIF3D/REBUS-3 calculation at EOC2 and will reflect the largest buildup of fission products.

Table 9 compares the components of the Na void reactivity effect at the EOC2 for the 20, 8, and 4 group cross section sets and shows the effect of the ENDF/B-IV vs. ENDF/B-V data bases. Sodium-voided cross sections were used in the appropriate reactor zones for these calculations. For comparison, the BOC1 Na void reactivity effect is also shown in Table 9. The impact of using sodium voided cross sections is also displayed. Using only non-voided cross sections results in about a 28¢ reduction in the total sodium reactivity.

The data of Table 9 show that fairly accurate sodium void reactivity worths can be calculated using very few energy groups. The difference between the four-group and twenty-group results is less than 40¢ out of a void worth of ~3.9$ at EOC2. The large change in void worth over the cycle ~1.5$, is a consequence of the long fuel residence times, 3 years, for the benchmark model. A very slight decrease in void worth, ~1%, is noted in going from ENDF/B-IV to ENDF/B-V data.

Table 9. Components of the Sodium Void[a] $\Delta k/kk^{*}$ [b]

	Spectral[c]	Total Non-Leakage	Leakage	Total
EOC2				
20 groups[e]	2.187-2[d]	1.896-2	-5.404-3	1.355-2
8 groups[e]	1.810-2	2.033-2	-7.465-3	1.287-2
4 groups[e]	1.591-2	1.998-2	-7.733-3	1.224-2
8 groups[f]	1.806-2	1.900-2	-7.112-3	1.188-2
8 groups[g]	1.797-2	2.114-2	-8.096-3	1.305-2
BOC1				
4 groups[e]	1.370-2	1.807-2	-1.092-2	7.082-3

[a] Na voided from drivers and upper axial blankets

[b] $\Delta k = k^{*} - k$, $k = k_{eff}$ from real non-voided calculation, k^{*} from adjoint voided calculation

[c] Group-to-group scattering component

[d] read as 2.187×10^{-2}

[e] Using the ENDF/B-V data base

[f] Using only non-voided sodium cross sections

[g] Using the ENDF/B-IV data base

SUMMARY AND CONCLUSIONS

In summarizing the results of any computational benchmark study it is necessary to qualify the conclusion with the caveat that they are applicable to the problem studied and it may not be possible to generalize. Nevertheless, the generic nature of the particular problem studied in this paper suggests that many of the results are quite generally applicable.

It was found that each of the three neutronics methodologies considered was capable of providing accurate fast reactor depletion results. Because of their relatively low computational costs, the nodal and synthesis methods make possible routine three-dimensional fast reactor depletion analysis. The nodal method would appear to be the more desirable of the two owing to its accuracy and ease of use.

The benchmark problem results showed that it is possible to obtain accurate depletion results using only four energy groups in the analysis. This conclusion, when coupled with the efficient neutronics methods discussed above, increases the feasibility of routine fast reactor three-dimensional analysis. The accuracy of the few-group results was apparent even for spectrum-sensitive parameters such as the sodium void effect. To ensure such accuracy considerable care is required in the preparation of such four-group constants. For example, spatial and spectral detail must be retained during the cross section generation.

The benchmark problem results also showed that control-rod position during the depletion cycle had very little impact on problem results. As a consequence of this conclusion, it is possible to perform the depletion analysis with control rods parked at the core-upper axial blanket interface throughout the burn cycle rather than finding an average control-rod position.

It was further found that the change in general purpose database from ENDF/B-IV to ENDF/B-V had very little impact on such integral parameters as reactivity swing, breeding ratio, power peaking, or sodium void worth. There was however a bias in eigenvalue (~.7%) between the two data bases.

APPENDIX A

PERFORMANCE COMPARISONS OF NEUTRONICS METHODS

Timing and cost comparisons between methods are always ambiguous, but nonetheless are always of interest. We quote three measures of performance for the 8-group reference calculations: CPU time for the BOC1 neutronics calculation, disk/core data transfers (in buffer loads) for the BOC1 neutronics calculation plus the first burn step, and dollar cost for the BOC1 neutronics calculation plus the first burn step.

Table A1 shows quantitative comparisons of performance. The results are given only relative to the performance of the finite-difference code, not in absolute terms. All SYN3D numbers contain a prorated contribution from the work required to generate the trial functions.

The nodal option in DIF3D currently runs only with all data for all groups core-contained; the finite-difference calculations were run in a mode which kept approximately half of the data for one group core-contained. As run, the nodal option required twice the core storage that the finite-difference option used. 90% of the CPU time required for a burnup calculation is spent in the neutronics module when the neutronics is finite-difference. For the nodal neutronics that figure is 73%. SYN3D/REBUS-3 is able to run efficiently at smaller core-storage allocations than were used, but no effort was made to optimize the runs. The nodal calculation will eventually offer data-management modes that will let it run with smaller core storage.

Table A1. Relative Performance Comparison of Neutronics Methods

Calculation	CPU	Disk/Core I/O	Core Storage	Cost
Finite-Difference	1.00	1.00	1.00	1.00
Nodal	.26	.09	2.23	.35
Flux Synthesis	.54	.21	.88	.39

REFERENCES

1. R. M. Wu, R. P. Omberg, R. Protsik, C. L. Cowan, J. W. Lewellen, ed., "The Large Core Code Evaluation Working Group Benchmark Analysis of a Heterogeneous Fast Reactor," DOE/TIC-2005709, January 1982.

2. D. R. Ferguson and K. L. Derstine, "Optimized Iteration Strategies and Data Management Considerations for Fast Reactor Finite Difference Diffusion Theory Codes," Nucl. Sci. Eng. 64, 593 (1977).

3. R. D. Lawrence, "A Nodal Interface Current Method for Multigroup Diffusion Calculations in Hexagonal Geometry," Trans. Am. Nucl. Soc. 39, 461 (1981).

4. C. H. Adams, "SYN3D: A Single Channel, Spatial Flux Synthesis Code for Diffusion Theory Calculations," ANL-76-21, July 1976.

5. C. H. Adams and W. M. Stacey, Jr., "Flux Synthesis Calculations for Fast Reactors," Nucl. Sci. Eng. 54, 201 (1974).

6. R. P. Hosteny, "The ARC System Fuel Cycle Analysis Capability, REBUS-2," ANL-7721, October 1978.

7. H. Henryson II, B. J. Toppel, and C. G. Stenberg, "MC^2-2: A Code to Calculate Fast Neutron Spectra and Multigroup Cross Sections," ANL-8144, June 1976.

8. B. J. Toppel, "The New Multigroup Cross Section Code MC^2-2," Proc. Conf. on New Applications in Reactor Mathematics and Applications, CONF-710302 (1971).

9. W. M. Stacey, Jr., B. J. Toppel, H. Henryson II, B. A. Zolotar, R. N. Hwang, and C. G. Stenberg, "A New Space-Dependent Fast-Neutron Multigroup Cross-Section Preparation Capability," Trans. Am. Nucl. Soc. 15, 292 (1972).

10. D. Garber, "ENDF-201, ENDF/B Summary Documentation," BNL 17541 (ENDF-201) 2nd Edition, Oct. 1975.

11. R. Kinsey, "ENDF-201, ENDF/B Summary Documentation ," BNL-NCS-17541 (ENDF-201) 3rd Edition, July 1979.

12. J. R. Liaw and H. Henryson II, "Lumped Fission Product Cross Sections from ENDF/B-V for Fast Reactor Analysis," Trans. Am. Nucl. Soc., 38, 657 (1981).

13. R. D. Lawrence, private communication.

14. To be published.